Periodica Polytechnica Mechanical Engineering, 69(4), pp. 318–328, 2025

Identification of the Transient Phase of Cutting by the Specific Cutting Force and Acoustic Emission During Metal Cutting

István Polyák[1*], István Biró[1], Tibor Szalay[1]

[1] Department of Manufacturing Science and Engineering, Faculty of Mechanical Engineering, Budapest University of Technology and Economics, Műegyetem rkp. 3., H-1111 Budapest, Hungary
[*] Corresponding author, e-mail: xpolyak@edu.bme.hu

Received: 10 June 2025, Accepted: 24 September 2025, Published online: 07 November 2025

Abstract

The stability of material processing during cutting concerns the continuity and coherence of the material processing conditions. A stable process results in predictable outputs such as cutting force and surface quality (roughness, integrity, texture). However, cutting processes encounter a transient phase before the cutting conditions reach their expected state. For example, during microcutting, material temporarily accumulates before the cutting edge is removed, resulting in outputs that differ significantly from what was anticipated. The aim of this paper is to provide a set of in-process parameters that can effectively indicate the transient phase of cutting. A statistical exploratory approach was utilized: face grooving tests were repeatedly conducted under the same nominal conditions and evaluated based on data deviation around the dataset's local mean. The specific cutting force and specific acoustic emission (AE) were chosen as indicative in-process parameters; additionally, the former is a common parameter used to describe the machinability of metal alloys, and the latter relates to the dynamic conditions (vibrations) of the material processing. The null hypothesis was that the specific cutting force and specific AE, as functions of the uncut chip thickness, have a uniform deviation from the predicted value within given ranges of the uncut chip thickness. A one-sample Student's t-statistic was performed on the datasets to assess the acceptability of the null hypothesis. Results of the t-statistic and the corresponding confidence intervals (CIs) indicate that there is a significant change in data distribution below what the literature describes as the minimum uncut chip thickness.

Keywords

t-statistic, face grooving, thin chip removal, machinability, specific acoustic emission, specific cutting force

1 Introduction

The demand for precision-machined products has increased. The industry is attempting to meet these demands while keeping manufacturing economical. By enhancing precision metal cutting, both precision and miniaturized part manufacturing can be achieved economically [1]. Challenges such as predicting conditions and maintaining the process stability of thin chip removal must be overcome to improve the precision and overall sustainability in part manufacturing through cutting [2, 3].

In our study, the stability of a cutting process relates to the continuity and coherence of the material processing conditions, i.e., a chip formation is considered stable if the dominant processing mechanism is the plastic deformation in a determinable shearing zone of the chip root without interruption. A stable process results in predictable outputs such as cutting force and surface quality (roughness, integrity, texture). However, cutting processes always experience a transient phase before the cutting conditions evolve to the defined state. For instance, when the cutting edge is only slightly in contact with the material, ploughing may temporarily become the dominant mechanism, resulting in outputs that differ significantly from those expected under stable conditions. Regardless of the cutting process type, a fundamental attribute is that the transient phase occurs under the conditions of thin chip removal. This transient phase arises, for example, during the end milling of a groove. Notably, the up-milling and down-milling sides of groove milling may yield fundamentally different surface quality, particularly in softer materials [4]. This highlights the importance of understanding the transient phase in cutting: due to the kinematics of groove milling, each edge of the milling cutter approaches and leaves the material with each tool rotation, meaning that every edge encounters the transient phase [5–7]. In fact, the surface

Cite this article as: Polyák, I., Biró, I., Szalay, T. "Identification of the Transient Phase of Cutting by the Specific Cutting Force and Acoustic Emission During Metal Cutting", Periodica Polytechnica Mechanical Engineering, 69(4), pp. 318–328, 2025. https://doi.org/10.3311/PPme.41227

quality of the groove wall is entirely an output of the periodic sequence of transient phases.

1.1 The transient phase of chip removal

The transient phase of cutting refers to the cutting condition that acts as a transition between chip removal (i.e., separation of a material layer due to the wedge effect induced by the cutting tool's edge [8–10]) and ploughing (i.e., local elastic deformation of the machined surface layer by the cutting tool's edge [11–13]). This phase occurs when the uncut chip thickness (h) increases from a nominal value of zero during the edge's entry or decreases to zero from a starting size. From the tool's point of view, this can be observed when the cutting edge plunges into or retracts from the machined material. Fig. 1 [14] illustrates the stages of how the material processing conditions change at the r_β cutting edge radius. When the edge plunges into the material, there is no material removal; the tool only elastically deforms the surface, which recovers to its original form after the tool passes (Fig. 1 (a)). As the uncut chip thickness increases, the tool begins to plastically deform and plough the surface (Fig. 1 (b)). This is followed by a transition phase. With the continued increase in chip thickness, chip formation with stabilized material flow in the chip root develops (Fig. 1 (c)).

Therefore, the transient phase is inevitably present in all cutting processes, especially during peripheral slab milling, where the tool's kinematics cause a periodically changing h [15–18], as shown in Fig. 2 [17]. This phenomenon has a greater impact on micromilling processes, where material accumulation at the cutting edge and material removal periodically alter [16].

The r_β cutting edge radius plays a significant role in these conditions: as the layer to be removed becomes thinner, the h/r_β ratio drops, resulting in an increasingly negative effective rake angle (γ_{eff}) of the tool, as illustrated in Fig. 1. A large negative rake angle produces high compressive stress in the cutting zone, which can lead to an unpredictable process due to material re-bump [19]. The machined surface in this region may exhibit irregularities; the ploughing and possible side flow can negatively affect the surface quality [20–22]. It also influences the degree of deformation beneath the machined surface [23–25].

The minimum uncut chip thickness (h_{min}), referred to as a limit, indicates the threshold below which no chip removal occurs with stabilized material flow; instead, the tool only deforms (i.e., ploughs) the machined surface elastically and plastically [26, 27]. Understanding the effect of r_β on material flow stability, h_{min} depends on r_β. This dependence is represented by the h_{min}/r_β ratio, which typically ranges between $h_{min}/r_\beta = 0.2$ and 0.4 [17, 28, 29]. As such, h_{min} can represent the upper limit of the transient phase of cutting.

In summary, understanding the transient phase of cutting leads to better predictability of cutting conditions when operating under the circumstances of thin chip removal. The attributes of the transient phase provide new insights into the machinability of various materials.

1.2 Studying and modelling the conditions of thin chip removal

Various practical methods are employed to study the thin chip removal. One major category consists of experimental studies performed with different chip removal technologies [30]. Another significant category is predictive simulation [31], which this paper does not explore further. In the experimental approach, researchers utilize several variables and indicative parameters.

One of the most common measurement methods is measuring the cutting force components that occur during the cutting process. The force measurement technique has been a well-established practice in traditional machining processes for decades [12–15, 17, 24–29, 32]. The specific cutting force is defined as the cutting force divided by the uncut chip section (i.e., the cross-section of the material layer to be removed; see Eq. (1)):

$$k_c(h) = \frac{F_c(h)}{h \cdot b}. \tag{1}$$

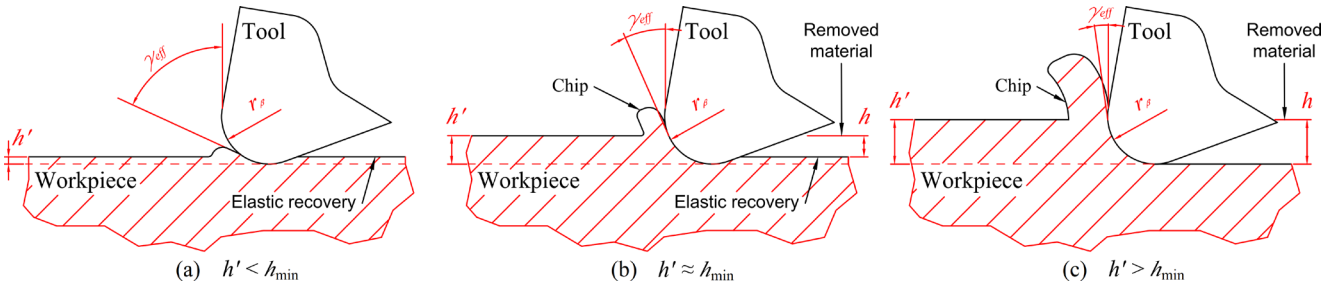

Fig. 1 Chip formation in the transient phase of cutting (adapted from [14]): (a) $h' < h_{min}$; (b) $h' \approx h_{min}$; (c) $h' > h_{min}$

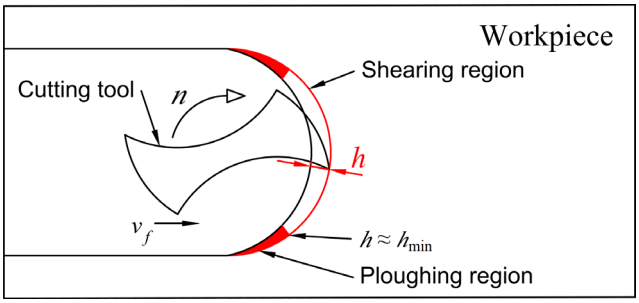

Fig. 2 Regions of chip formation in micromilling (adapted from [17])

When the specific cutting force is plotted as a function of the uncut chip thickness, it can be approximated by an exponential curve (see Eq. (2)), which represents the Kienzle-type modeling approach, also known as the inverse power law model [32]:

$$k_c(h) = k_{c1} \cdot h^{-m}, \tag{2}$$

where k_{c1} is a material constant, and m represents the size effect component.

Another measurement method that characterizes the material formation process from an energetic point of view is the method of measuring internal acoustic emission (AE). This method provides a pressure wave-type signal that is proportional to the degree of material deformation (lattice distortion, dislocation movement, or simply internal and external friction between surfaces), which propagates through both the machined material and the machining tool [33]. Like force measurement, it can be converted into an analog voltage with a piezoelectric measuring device and subsequently into a digital signal. The AE signal is an indicator with low energy content and a frequency characteristic in the ultrasonic range. Its recording and sampling demand special equipment. Consequently, the examination of AE root mean square (AE_{RMS}) is widely conducted, which can be produced with a similar method by integrating the voltage signal [33].

Since the extent of AE depends on the intensity of deformation, i.e., the area of layer cross-section deformation during chip formation, it is also well-suited for examining the energetics in the transient stage of cutting. Although less common in the literature, it also occurs in a form specific to the chip cross-section (specific AE_{RMS} [33–35]). Its value (*ae*) can be calculated using an expression (Eq. (3)) similar to the specific cutting force (Eq. (1)):

$$ae(h) = \frac{AE_{RMS}(h)}{h \cdot b}, \tag{3}$$

$$ae(h) = ae_1 \cdot h^{-m_{ae}}. \tag{4}$$

At the tool edge entry, the characteristics of the specific quantities mentioned deviate from the traditional exponential mathematical model. During repeated yet variable factor measurements, a similar phenomenon can be observed in the diagrams of the specific values interpreted as a function of chip thickness. Researchers examine this characteristic using various methods. One such method [36] involves dividing the process indicator into stages based on the dominant chip formation mechanism. The division into four stages is interpreted as follows:

- macro chip removal $h >= 0.1$ mm;
- fine chip removal $0.01 =< h < 0.1$ mm;
- micro-scale chip removal $0.003 =< h < 0.01$ mm;
- micro-chip removal with increased size effect due to ploughing $h < 0.003$.

The presented research aims to investigate the uncertainty with which the specific process characteristics (depending on the chip thickness) can be determined. Only in certain cutting technologies is it feasible to measure specific parameters, including the thickness of the material removed. Traditional techniques like milling, drilling, and longitudinal turning only provide an estimate of the thickness of the material removed. This estimate is usually based on a theoretical chip cross-section calculated through established models. On the other hand, methods that utilize linear main cutting motion, such as chiseling and planing, allow for direct measurement of the theoretical chip cross-section. However, these technologies have significant limitations when it comes to the cutting speeds that can be used. To overcome these challenges, we conducted face-grooving turning experiments [37], which allow for high accuracy in determining the removed layer thickness afterward. The experimental settings were repeated eight times using the same parameters to ensure repeatability. Subsequently, the examined parameters, their uncertainty, and statistical behavior were analyzed using t-statistical methods.

2 Experiment and measurements

As part of an investigation, a set of face grooving turning tests was conducted (see Fig. 3 [38]). During the experiment, the groove was formed along a three-quarter arc (see Fig. 4), allowing the measurement of groove depth afterwards. A total of eight partial grooves were created on the disc-shaped specimen. The eight measurements vary only in terms of the machining diameter. However, the investigation of how the machining diameter affects the deviation from free cutting is not included in the current

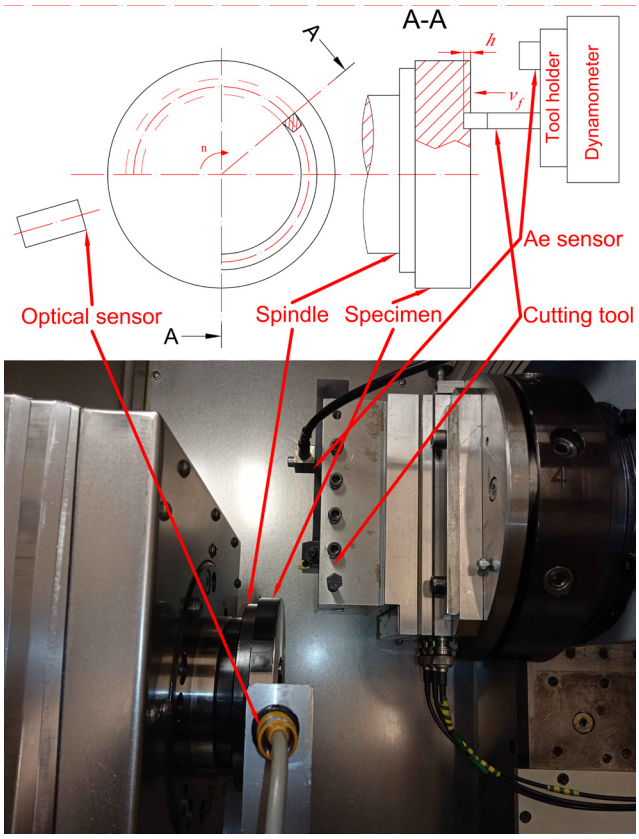

Fig. 3 Experimental setup (adapted from [38])

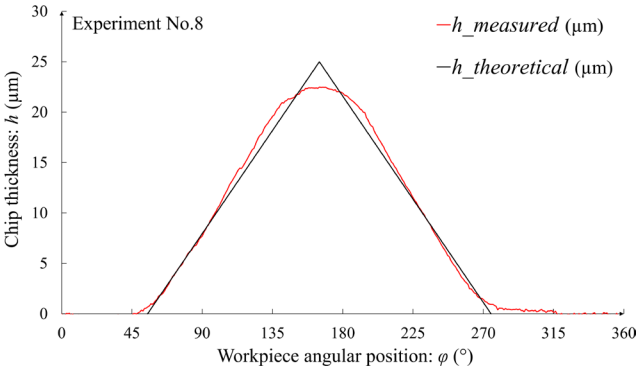

Fig. 4 Theoretical and evaluated chip thickness

research presented here. Due to the cutting arrangement, the thickness and width of the separated layer can be directly equated to the uncut chip thickness (h) and the uncut chip width (b), respectively (see Fig. 5). The thickness of the cross-section of the separated layer does not align with the theoretical (or programmed) uncut chip thickness (h'). The chip thickness exhibits a non-linear characteristic at both the entry and exit of the tool edge. This is primarily due to the localized elastic deformation of the machined surface, which is significant during thin chip removal compared to the theoretical chip thickness. The elastic deformation of the machining environment also contributes to this effect. Considering the low load of the machine tool and its robust design, the latter factor is negligible.

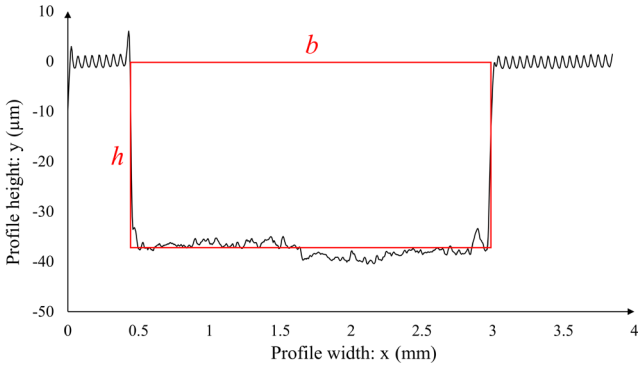

Fig. 5 Measured profile and evaluated theoretical chip geometry

The experiment was conducted in the ultra-precision and micro-machining laboratory of the Department of Manufacturing Science and Technology at Budapest University of Technology, using a Hembrug Mikroturn 50 (Gipuzkoa, Spain) precision lathe. The specimen was made of S960QL, high-strength structural steel. The cutting tool (Seco 10EAL2.5FA) had a carbide (Seco CP500 grade) insert with a (Ti, Al) N + TiN coating, suitable for machining superalloys. An optical microscope was utilized to measure the cutting edge radius, which was $r_\beta = 20$ µm. The tool was mounted on a piezoelectric dynamometer (Kistler 9257A, Prague, Czech Republic), and the AE sensor (Kistler 8152B221, Prague, Czech Republic) was attached to the tool holder. With the aid of an optical sensor (Omron E3F-DS10B4, Tokyo, Japan), we determined the precise period of the specimen's rotation. This ensures that the profile measurement after the process, conducted with a Mitutoyo SJ 400 (Neuss, Germany) device, and the in-process measurements can be synchronized. Consequently, the specific cutting force and specific AE values can be precisely determined. The technological parameters were settled through the eight experiments, during which a cutting speed of $v_c = 120$ m/min and a feed rate of $v_f = 50$ mm/min were used. The nominal groove width was $b' = 1$ mm, and the maximum nominal groove depth was $h' = 25$ µm. The graphs of the measurements are in Fig. A1 to A8 in Appendix A.

3 Results and discussion

The evaluation occurred in the LabVIEW 2022 software [39] environment. We derived the uncut chip thickness and uncut width of the chip from the profile measurement data. The automatic evaluation algorithm sequentially extracts profile measurement data. Throughout the evaluation process, the prepared front surface serves as the reference point ($h = 0$ µm). This is accomplished by averaging the profile measurement values from both the first and last

10% of the data in the measurement series. The edge of the groove is identified by locating a local minimum value that is at least 50% lower than the minimum value of the reference point. The distance between the edges of the groove can be regarded as equivalent to the width of the deformed layer. Furthermore, the thickness of the deformed layer can be approximated by taking the average of the measurement points situated between the edges of the groove. By combining these values with the in-process measurement data, we calculated the specific cutting force (Eq. (1)) and the specific AE (Eq. (4)) using the provided formulas. As we examined both specific values separately, using the same method, their values are denoted as $y(h)$ in Eq. (5):

$$y(h) = \begin{cases} k_c(h) & \text{for specific cutting force} \\ a_e(h) & \text{for specific cacoustic emission} \end{cases}. \tag{5}$$

Each of the eight experimental sets was analyzed separately. We employed an exponential curve-fitting method similar to the traditional Kienzle-Victor model. To achieve this, we linearized the samples using a logarithmic transformation (Eqs. (6) and (7)). A linear fit (Eq. (8)) was performed using the least squares method. The coefficients for the linear regressions can be found in Table A1 in Appendix A.

$$Y_i(h_i) = \log\left(y_i(h_i)\right) \tag{6}$$

$$H_i = \log(h_i) \tag{7}$$

$$Y_i(H_i) = A \cdot H_i + B \tag{8}$$

$$y_i(h_i) = 10^{Y_i(h_i)} \tag{9}$$

The fitted curve was converted back to the linear scale using Eq. (9) to analyze the statistical behavior of the sample relative to the fitted curve (i.e., the expected value). Each experiment's sample was divided into equal-width ranges of $h = 1$ µm, resulting in a total of 20 ranges (Fig. 6). The index $j = 1 \ldots 20$ refers to the serial number of the specified range in the formulas. The behavior of samples within these ranges was assessed using Student's t-statistics. The t-statistic quantitatively measures how much the sample's estimated value deviates from its expected value. It is primarily used in hypothesis testing, such as the t-statistic, particularly when the sample size is small and the population standard deviation is unknown.

$$s = \sqrt{\frac{1}{n-1}\sum_{i=0}^{n}\left(y_i - \bar{y}\right)^2} \tag{10}$$

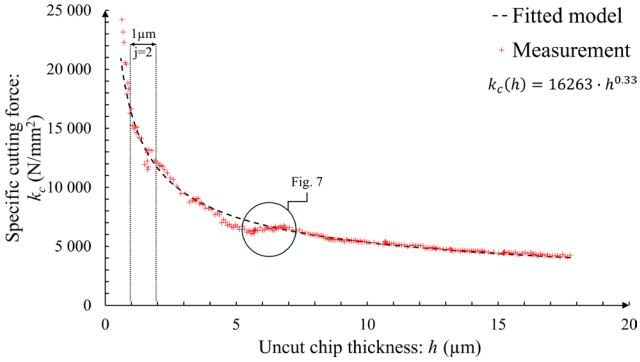

Fig. 6 Measured specific cutting force and the fitted inverse power law model for experiment No.8

$$\hat{\mu} = \frac{1}{n}\sum_{i=0}^{n}\left(y_i - \bar{y}\right) \tag{11}$$

$$\mu \in \left[\mu_U = \hat{\mu} - t_{n-1,1-\frac{\alpha}{2}}\frac{s}{\sqrt{n}};\ \mu_L = \hat{\mu} + t_{n-1,1-\frac{\alpha}{2}}\frac{s}{\sqrt{n}}\right] \tag{12}$$

$$\mathrm{CI}_{res.} = \frac{\mu_U + \mu_L}{2} \tag{13}$$

$$\mathrm{CI}_{rel.res.} = \frac{\mathrm{CI}_{res.}}{\bar{y}} \tag{14}$$

In our examination, the sample size for each range is fewer than ten ($n < 10$). We also assume that any unknown error in the measurements follows a normal standard distribution. The unknown population standard deviation can be approximated by the corrected standard deviation of the sample (Eq. (10)). The deviation of the measurement points from the expected value can be calculated using Eq. (11). With this in mind, a 95% confidence interval (CI) was calculated to estimate the true population mean (Eq. (12)), where μ_U stands for the upper boundary and μ_L for the lower boundary of the CI. The location of the CI relative to the expected value and its width provides statistically valuable information for regression analysis. The average deviation of the CI (namely $\mathrm{CI}_{res.}$) over the given h-range can be calculated using Eq. (13) (see Fig. 7). For comparability, we performed dimensionless analysis, determining the relative deviation from the expected value (Eq. (14)). The value of $\mathrm{CI}_{rel.res.}$ for both specific values as a function of the uncut chip thickness is shown in the diagram (Fig. 8).

Considering all eight measurements, we observed that this quantity switched signs multiple times within the studied range of uncut chip thickness ($0.5 < h < 20$ µm). As h decreases, it tends to take on larger values, suggesting that the regression used to determine the expected val-

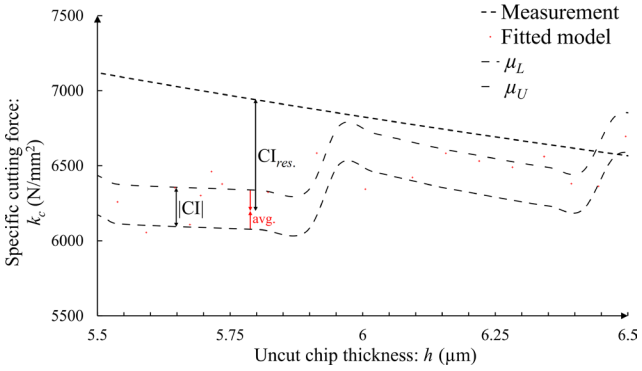

Fig. 7 Residuum of CI from the expected value and width of the CI

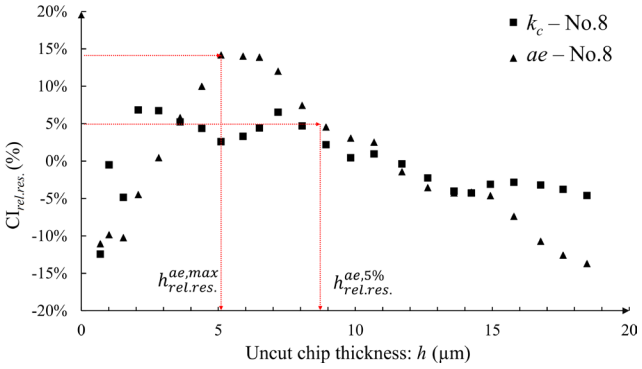

Fig. 8 Relative residuum of the CI for experiment No.8

ue offers a less accurate prediction for the measurement. The ± values presented in the quantities below indicate the standard deviations for the entire experimental series.

In the case of the specific cutting force, there is a local minimum of:

- $CI^{k_c,l.min}_{rel.res.} = -6.7 \pm 5.4(\%)$ at the value of
- $h^{k_c,l.min}_{rel.res.} = 5.34 \pm 0.85(\mu m)$.

In the case of the specific AE, there is a local maximum:

- $CI^{ae,max}_{rel.res.} = 11.6 \pm 4.0(\%)$, in the same range,
- $h^{ae,max}_{rel.res.} = 4.39 \pm 1.33(\mu m)$.

These values are found at:

- $h^{k_c,l.min}_{rel.res.} / r_\beta = 0.27 \pm 0.04(1)$ and
- $h^{ae,max}_{rel.res.} / r_\beta = 0.22 \pm 0.07(1)$ relative to the tool edge radius. This range is below the usual range of the minimum uncut chip thickness. The values are broken down into individual experiments, which can be found in Table 1.

In the case of specific cutting force, $CI^{k_c,5\%}_{rel.res.}$ reaches a relative error limit of 5% in the range of:

- $h^{k_c,5\%}_{rel.res.} = 9.33 \pm 4.7(\mu m)$, and for specific AE, it is at
- $h^{ae,5\%}_{rel.res.} = 6.78 \pm 2.4(\mu m)$ on average during the measurements. These values are found at
- $h^{k_c,5\%}_{rel.res.} / r_\beta = 0.47 \pm 0.24(1)$ and
- $h^{ae,5\%}_{rel.res.} / r_\beta = 0.34 \pm 0.12(1)$ concerning the tool nose radius. This range is below the typical minimum uncut chip thickness range and sits at the lower limit of its usual range.

$$|CI|_{rel.} = \frac{2 \cdot t_{n-1,1-\frac{\alpha}{2}} \frac{s}{\sqrt{n}}}{\bar{y}} \tag{15}$$

Another key statistical characteristic, the width of the CI, is influenced by sample size and variance. In this study, we maintain a significance level of 95%. We also examined its value after standardizing with the expected value, which is calculable using Eq. (15). The resulting values $(|CI|_{rel.})$ are depicted in Fig. 9 for the 8th measurement. Results from the other measurements are presented in Appendix A. This quantity also indicates, that as the uncut chip thickness (h) decreases, it tends to take on larger values, suggesting instability in the process. In the

Table 1 Summary of results for the set of experiments

Value	Unit	No.1	No.2	No.3	No.4	No.5	No.6	No.7	No.8	Avg.	St.dev. (s)	h/r_β	s/r_β
$CI^{k_c,5\%}_{rel.res.,j}$	%	5	5	5	5	5	5	5	5	5	–	–	–
$h^{k_c,5\%}_{rel.res.,j}$	µm	14.86	6.17	5.32	6.29	18.03	6.07	10.01	7.92	9.33	4.70	0.47	0.24
$CI^{ae,5\%}_{rel.res.,j}$	%	5	5	5	5	5	5	5	5	5	–	–	–
$h^{ae,5\%}_{rel.res.,j}$	µm	7.29	6.16	7.23	1.18	7.24	8.28	8.77	8.06	6.78	2.40	0.34	0.12
$CI^{k_c,l.min}_{rel.res.,j}$	%	−11.4	−5.0	−9.0	−7.0	0.4	−12.3	−10.2	2.6	−6.7	5.4	–	–
$h^{k_c,l.min}_{rel.res.,j}$	µm	6.46	6.16	4.33	6.06	4.60	5.57	4.41	5.10	5.34	0.85	0.27	0.04
$CI^{ae,max}_{rel.res.,i}$	%	18.6	11.4	9.0	4.9	12.9	10.1	11.6	14.2	11.6	4.0	–	–
$h^{ae,max}_{rel.res.,j}$	µm	2.82	3.33	4.33	2.81	4.60	6.11	6.06	5.10	4.39	1.33	0.22	0.07
$\|CI\|^{k_c,5\%}_{rel.,j}$	%	5	5	5	5	5	5	5	5	5	–	–	–
$h^{k_c,5\%}_{rel.,j}$	µm	2.64	1.50	3.35	1.63	4.08	4.33	3.56	2.75	2.98	1.05	0.15	0.05
$\|CI\|^{ae,5\%}_{rel.,j}$	%	5	5	5	5	5	5	5	5	5	–	–	–
$h^{ae,5\%}_{rel.,j}$	µm	1.67	0.90	1.03	1.10	1.26	1.06	1.51	0.69	1.15	0.32	0.06	0.02

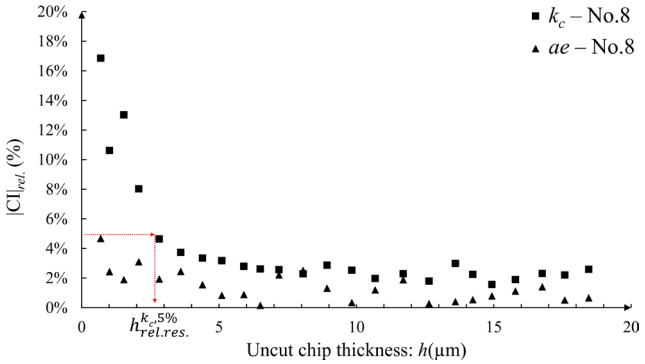

Fig. 9 Width of the CI for experiment No.8

case of specific cutting force, the relative CI width reaches a relative difference limit of 5% $\left(|CI|_{rel.}^{k_c,5\%}\right)$ in the range:

- $h_{rel.res.}^{k_c,5\%} = 2.98 \pm 1.05(\mu m)$, and for specific AE $\left(|CI|_{rel.}^{ae,5\%}\right)$, it is
- $h_{rel.res.}^{ae,5\%} = 1.15 \pm 0.32(\mu m)$ on average across the eight set of experiment. These values are found at
- $h_{rel.}^{k_c,5\%} / r_\beta = 0.15 \pm 0.05(1)$ and
- $h_{rel.}^{ae,5\%} / r_\beta = 0.06 \pm 0.02(1)$ relative to the tool edge radius, which range is much further away from the lower limit of the minimum uncut chip thickness range.

Our statistical analysis shows that the uncut chip thickness quantities represent the technological limit for conventional or macro chip removal, which the classical exponential formula can approximate. However, the statistical behavior of the process characteristics changes below this uncut chip thickness. As a result, we suggest modifying or correcting the model to ensure the expected value matches the measured values. Such correction can be done by adding a correction part to the mathematical model [40], or by using advanced functions.

4 Conclusions

Using the one-sample Student's t-statistic, we confirmed that the distribution behavior of the measured specific cutting force and specific AE changes as the uncut chip thickness approaches zero. By fitting the measured data with the exponential model and then analyzing the deviation of the data from the model in sets, we can state the following:

- The statistical behavior, quantified with the CI, of the sample changes in the range below $h < 1.3$ µm, as evidenced by the diagram (see Figs. 7 and 8).
- The approximating exponential model, such as the Kienzle-Victor model, requires adjustment in the range where the sample exhibits different statistical behavior.

The uncut chip thickness quantities determined during the presented statistical evaluation indicate the technological limit of conventional or macro chip removal, which the classical exponential formula can approximate. The statistical behavior of the examined process characteristics changes in the range below this uncut chip thickness. Therefore, we recommend modifying or correcting the model so that the expected value determined by the model aligns with the measured values. Extending the technological model to include the range of thin chip thicknesses allows for further optimization in various chip removal technologies, such as micromilling. By broadening the examined range of the chip formation process, technological modifications, such as special toolpaths, can be established with greater certainty, which can enhance both the quality of the machined surface and the expected tool life. This allows the machining process to be planned with reduced energy investment and a focus on sustainability. To finalize the suggested correction for practical application, it is essential to replicate the experiments described here and widen the range of test variables. Future studies should concentrate on assessing the impact of technological parameters such as cutting speed and feed rate. Additionally, other variables can be incorporated, but this must be approached with caution due to the significant increase in resource demands for experimentation.

Acknowledgments

The project supported by the Doctoral Excellence Fellowship Programme (DCEP) is funded by the National Research Development and Innovation Fund of the Ministry of Culture and Innovation and the Budapest University of Technology and Economics, under a grant agreement with the National Research, Development and Innovation Office and partly supported by the National Research, Development and Innovation Office in the frame of the grant SNN146940 (Basic Investigation of the Applicability of Artificial Intelligence Based Predictive Models to Improve the Quality of Production with Advanced Machining Processes).

References

[1] Georgakopoulos-Soares, I., Papazoglou, E. L., Karmiris-Obratański, P., Karkalos, N. E., Markopoulos, A. P. "Surface antibacterial properties enhanced through engineered textures and surface roughness: A review", Colloids and Surfaces B: Biointerfaces, 231, 113584, 2023. https://doi.org/10.1016/j.colsurfb.2023.113584

[2] Kundrák, J., Fedorovich, V., Markopoulos, A. P., Pyzhov, I., Ostroverkh, Y. "Increasing the reliability of a bladed tool made from synthetic polycrystalline diamonds", International Journal of Refractory Metals and Hard Materials, 110, 106045, 2023. https://doi.org/10.1016/j.ijrmhm.2022.106045

[3] Tancsa, V., Jacso, A., Poka, G. "Lamé Curve-based Spiral Tool Path Generation for Rough Milling", Periodica Polytechnica Mechanical Engineering, 69(3), pp. 259–273, 2025. https://doi.org/10.3311/PPme.41247

[4] Diez, E., Perez, H., Marquez, J., Vizan, A. "Feasibility study of in-process compensation of deformations in flexible milling", International Journal of Machine Tools and Manufacture, 94, pp. 1–14, 2015. https://doi.org/10.1016/j.ijmachtools.2015.03.008

[5] Karmiris-Obratański, P., Karkalos, N. E., Kudelski, R., Markopoulos, A. P. "Experimental study on the effect of the cooling method on surface topography and workpiece integrity during trochoidal end milling of Incoloy 800", Tribology International, 176, 107899, 2022. https://doi.org/10.1016/j.triboint.2022.107899

[6] Mgherony, A., Mikó, B., Farkas, G. "Comparison of Surface Roughness When Turning and Milling", Periodica Polytechnica Mechanical Engineering, 65(4), pp. 337–344, 2021. https://doi.org/10.3311/PPme.17898

[7] Borysenko, D., Karpuschewski, B., Welzel, F., Kundrák, J., Felhő, C. "Influence of cutting ratio and tool macro geometry on process characteristics and workpiece conditions in face milling", CIRP Journal of Manufacturing Science and Technology, 24, pp. 1–5, 2019. https://doi.org/10.1016/j.cirpj.2018.12.003

[8] Hao, Z., Cheng, G., Fan, Y. "Dynamic plastic evolution mechanism in cutting zone of nickel-based superalloy GH4169", Journal of Materials Processing Technology, 313, 117858, 2023. https://doi.org/10.1016/j.jmatprotec.2023.117858

[9] Altan, E., Emiroğlu, U. "New slip-line field model based on dead metal zone and material flow in negative rake orthogonal cutting", Journal of the Brazilian Society of Mechanical Sciences and Engineering, 44(10), 445, 2022. https://doi.org/10.1007/s40430-022-03758-7

[10] Merchant, M. E. "Mechanics of the Metal Cutting Process. I. Orthogonal Cutting and a Type 2 Chip", Journal of Applied Physics, 16(5), pp. 267–275, 1945. https://doi.org/10.1063/1.1707586

[11] Wen, D.-Y., Wan, M., Linghu, S.-C., Zhang, W.-H. "A slip-line field model for independently characterizing shearing and ploughing effects in metal cutting processes", Wear, 556–557, 205504, 2024. https://doi.org/10.1016/j.wear.2024.205504

[12] Wen, D.-Y., Wan, M., Ren, Y.-Y., Zhang, W.-H., Yang, Y. "Material piling up and spreading effects in the cutting processes with small feed rates", Mechanical Systems and Signal Processing, 171, 108839, 2022. https://doi.org/10.1016/j.ymssp.2022.108839

[13] Albrecht, P. "New Developments in the Theory of the Metal-Cutting Process: Part I. The Ploughing Process in Metal Cutting", Journal of Manufacturing Science and Engineering, 82(4), pp. 348–357, 1960. https://doi.org/10.1115/1.3664242

[14] Aramcharoen, A., Mativenga, P. T. "Size effect and tool geometry in micromilling of tool steel", Precision Engineering, 33(4), pp. 402–407, 2009. https://doi.org/10.1016/j.precisioneng.2008.11.002

[15] Cappellini, C., Abeni, A. "An analytical micro-milling force model based on the specific cutting pressure-feed dependence, in presence of ploughing and tool run-out effects", Journal of Manufacturing Processes, 116, pp. 224–245, 2024. https://doi.org/10.1016/j.jmapro.2024.02.057

[16] Lyu, W., Liu, Z., Liang, X., Wang, B., Cai, Y. "A novel analytical model for predicting ploughing effect on machined wall surface topography considering tool wear during slot milling process", Journal of Manufacturing Processes, 127, pp. 9–26, 2024. https://doi.org/10.1016/j.jmapro.2024.07.109

[17] Sahoo, P., Patra, K., Szalay, T., Dyakonov, A. A. "Determination of minimum uncut chip thickness and size effects in micro-milling of P-20 die steel using surface quality and process signal parameters", The International Journal of Advanced Manufacturing Technology, 106(11), pp. 4675–4691, 2020. https://doi.org/10.1007/s00170-020-04926-6

[18] Zhanqiang, L., Zhenyu, S., Yi, W. "Definition and determination of the minimum uncut chip thickness of microcutting", The International Journal of Advanced Manufacturing Technology, 69(5), pp. 1219–1232, 2013. https://doi.org/10.1007/s00170-013-5109-4

[19] Elsanabary, S., Elkaseer, A., Abd-Rabbo, S., AbdElsalam, M., Abdou, S. "Surface generation in ultra-precision turning considering process uncertainty: Modeling and experimental validation", In: Proceedings of the 17th International Conference on Applied Mechanics and Mechanical Engineering, Cairo, Egypt, 2016, pp. 142–154. ISBN 9798331302184 [online] Available at: https://www.researchgate.net/publication/332098122_Surface_Generation_in_Ultra-Precision_Turning_Considering_Process_Uncertainty_Modeling_and_Experimental_Validation [Accessed: 20 September 2025]

[20] de Oliveira, D., Ziberov, M., de Paiva, R. L., da Silva, M. B. "An experimental evaluation of cutting parameters influence on the surface integrity and tool wear mechanisms on the dry micro-milling of austenitic alloy Inconel 718", Wear, 571, 205789, 2025. https://doi.org/10.1016/j.wear.2025.205789

[21] Zhang, L., Li, S., Li, L., Wei, C., Pan, P., Wang, J., Wan, Y., Peng, C., Hao, X. "Study on the influence of PCD micro milling tool edge radius on the surface quality of deep and narrow grooves", Journal of Manufacturing Processes, 131, pp. 1–11, 2024. https://doi.org/10.1016/j.jmapro.2024.09.013

[22] Xue, Z., Lai, M., Xu, F., Fang, F. "Influence factors and prediction model of surface roughness in single-point diamond turning of polycrystalline soft metal", Journal of Materials Processing Technology, 324, 118256, 2024. https://doi.org/10.1016/j.jmatprotec.2023.118256

[23] Elsheikh, A. H., Shanmugan, S., Muthuramalingam, T., Thakur, A. K., Essa, F. A., Ibrahim, A. M. M., Mosleh, A. O. "A comprehensive review on residual stresses in turning", Advances in Manufacturing, 10(2), pp. 287–312, 2022. https://doi.org/10.1007/s40436-021-00371-0

[24] Tang, Z., Huang, C., Shi, Z., Li, B., Liu, H., Niu, J., Chen, Z., Jiang, G. "A new characterisation method for stress, hardness, microstructure, and slip lines using the stored energy field in the cutting deformation zones of workpiece", International Journal of Machine Tools and Manufacture, 178, 103891, 2022. https://doi.org/10.1016/j.ijmachtools.2022.103891

[25] Zhang, P., Zhang, S., Wang, S., Sun, Y., Yue, X. "Construction of a predictive model for residual stresses in micro-milling of 7075 aluminum alloy", The International Journal of Advanced Manufacturing Technology, 131(7), pp. 3871–3883, 2024. https://doi.org/10.1007/s00170-024-13239-x

[26] Dib, M. H. M., Duduch, J. G., Jasinevicius, R. G. "Minimum chip thickness determination by means of cutting force signal in micro endmilling", Precision Engineering, 51, pp. 244–262, 2018. https://doi.org/10.1016/j.precisioneng.2017.08.016

[27] Li, T., Peng, B., Wu, W., Wang, P., Wang, Z., Zhu, Y. "Minimum cutting thickness prediction model for micro-milling machining and experimental Study of FeCoNiCrMn high-entropy alloy machining", Precision Engineering, 89, pp. 338–348, 2024. https://doi.org/10.1016/j.precisioneng.2024.06.021

[28] Yao, Y., Zhu, H., Huang, C., Wang, J., Zhang, P., Yao, P., Wang, X. "Determination of the minimum chip thickness and the effect of the plowing depth on the residual stress field in micro-cutting of 18 Ni maraging steel", The International Journal of Advanced Manufacturing Technology, 106(1), pp. 345–355, 2020. https://doi.org/10.1007/s00170-019-04439-x

[29] Aslantas, K., Hopa, H. E., Percin, M., Ucun, İ., Çicek, A. "Cutting performance of nano-crystalline diamond (NCD) coating in micro-milling of Ti6Al4V alloy", Precision Engineering, 45, pp. 55–66, 2016. https://doi.org/10.1016/j.precisioneng.2016.01.009

[30] Wojciechowski, S. "Estimation of Minimum Uncut Chip Thickness during Precision and Micro-Machining Processes of Various Materials—A Critical Review", Materials, 15(1), 59, 2022. https://doi.org/10.3390/ma15010059

[31] Wang, L., Yue, C., Liu, X., Li, M., Xu, Y., Liang, S. Y. "Conventional and micro scale finite element modeling for metal cutting process: A review", Chinese Journal of Aeronautics, 37(2), pp. 199–232, 2024. https://doi.org/10.1016/j.cja.2023.03.004

[32] Kienzle, O. "Die Bestimmung von Kräften und Leistungen an spänenden Werkzeugen und Werkzeugmaschinen" (Determination of forces and productivity of tools used for machine-tools), VDI-Z, 94(11), pp. 299–305, 1952. (in German)

[33] Mian, A. J., Driver, N., Mativenga, P. T. "Identification of factors that dominate size effect in micro-machining", International Journal of Machine Tools and Manufacture, 51(5), pp. 383–394, 2011. https://doi.org/10.1016/j.ijmachtools.2011.01.004

[34] Liu, J., Jiang, C., Yang, X., Sun, S. "Review of the Application of Acoustic Emission Technology in Green Manufacturing", International Journal of Precision Engineering and Manufacturing-Green Technology, 11(3), pp. 995–1016, 2024. https://doi.org/10.1007/s40684-023-00557-w

[35] Mian, A. J., Driver, N., Mativenga, P. T. "Chip formation in microscale milling and correlation with acoustic emission signal", The International Journal of Advanced Manufacturing Technology, 56(1), pp. 63–78, 2011. https://doi.org/10.1007/s00170-011-3185-x

[36] Biró, I., Szalay, T. "Extension of empirical specific cutting force model for the process of fine chip-removing milling", The International Journal of Advanced Manufacturing Technology, 88(9), pp. 2735–2743, 2017. https://doi.org/10.1007/s00170-016-8957-x

[37] Ramos, A. C., Autenrieth, H., Strauß, T., Deuchert, M., Hoffmeister, J., Schulze, V. "Characterization of the transition from ploughing to cutting in micro machining and evaluation of the minimum thickness of cut", Journal of Materials Processing Technology, 212(3), pp. 594–600, 2012. https://doi.org/10.1016/j.jmatprotec.2011.07.007

[38] Biró, I. "A forgácsleválasztás energetikai modelljének kiterjesztése nagy szilárdságú acél precíziós és mikroforgácsolási technológiájához" (Extension of the energy consumption model of mechanical chip-removal for precision and microcutting processes), PhD Thesis, Budapest University of Technology and Economics, 2017. [online] Available at: https://repozitorium.omikk.bme.hu/handle/10890/5479 [Accessed: 22 August 2022]

[39] National Instruments "LabVIEW 2022 Q3, (22.3)", [computer program] Available at: https://www.ni.com/en/support/downloads/software-products/download.labview.html?srsltid=AfmBOoo01077wuLIFF9R3UdiZoW5PzcRBcmzeghwf1-yHnfNrsH8nk9G#460283 [Accessed: 23 September 2025]

[40] Piquard, R., Thibaud, S., D'Acunto, A., Fontaine, M., Dudzinski, D. "Phenomenological modelling of micro-cutting based on experimental results", The International Journal of Advanced Manufacturing Technology, 88(9), pp. 3429–3436, 2017. https://doi.org/10.1007/s00170-016-9047-9

Appendix A

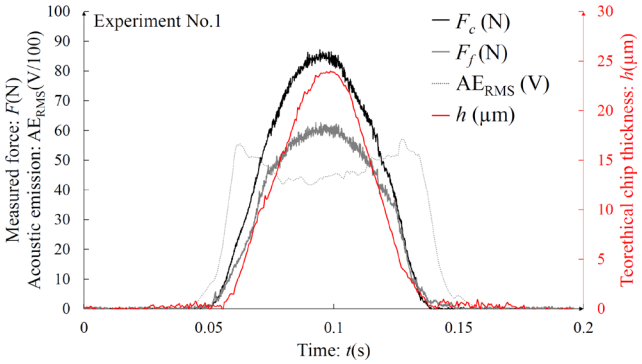

Fig. A1 Measurements for experiment No.1

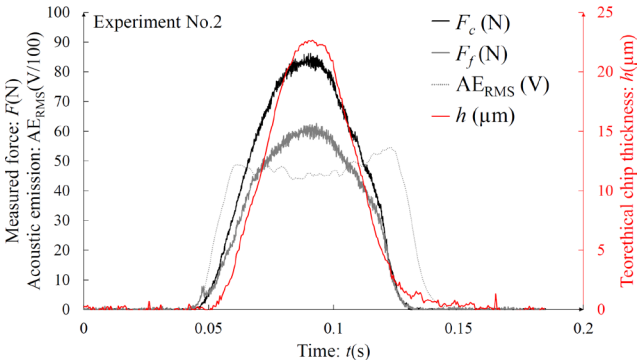

Fig. A2 Measurements for experiment No.2

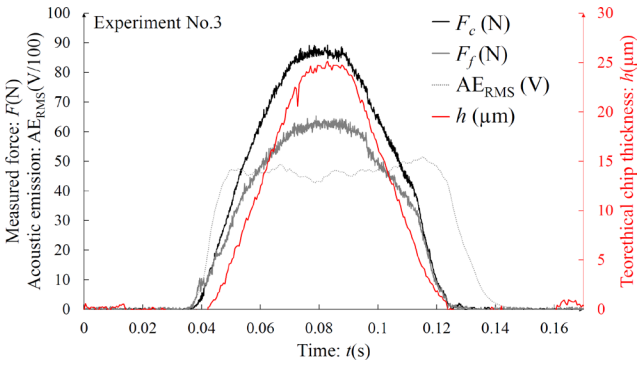

Fig. A3 Measurements for experiment No.3

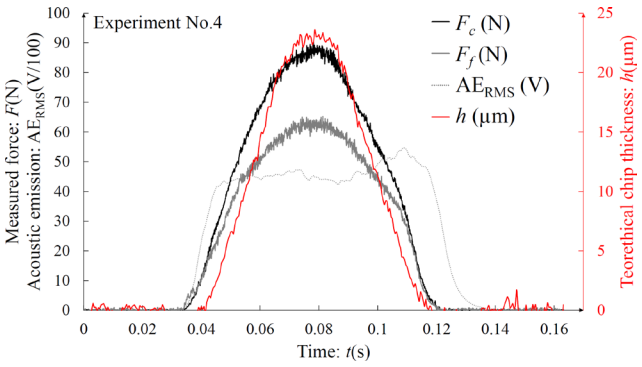

Fig. A4 Measurements for experiment No.4

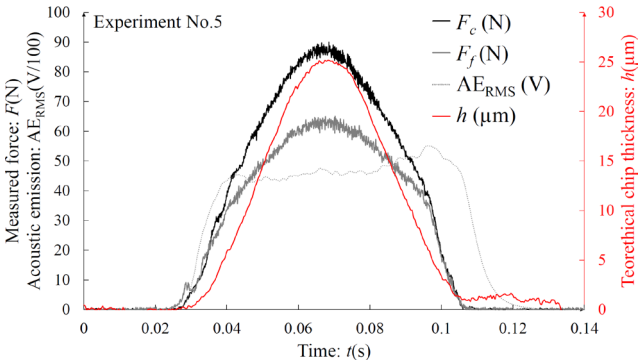

Fig. A5 Measurements for experiment No.5

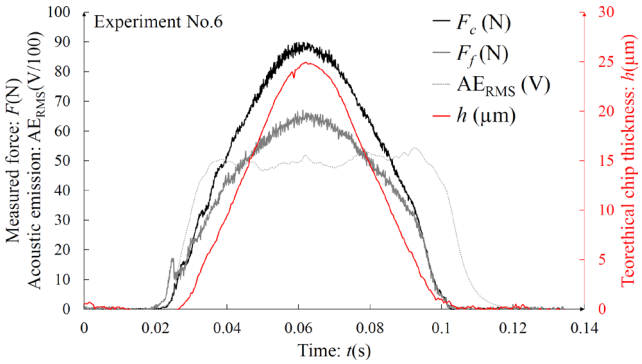

Fig. A6 Measurements for experiment No.6

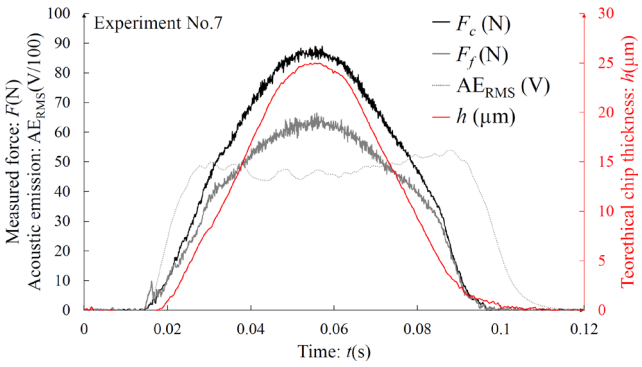

Fig. A7 Measurements for experiment No.7

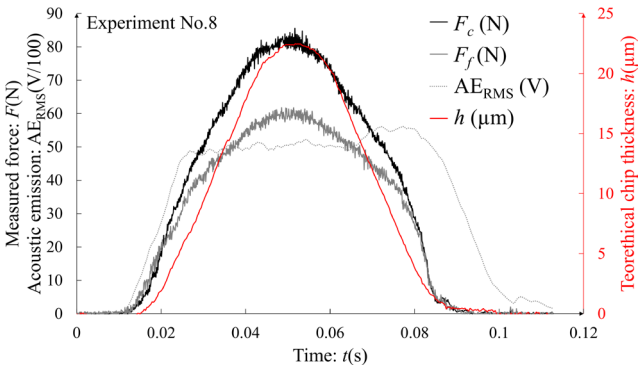

Fig. A8 Measurements for experiment No.8

Table A1 Coefficients obtained during linear regression

Coefficient	No.1	No.2	No.3	No.4	No.5	No.6	No.7	No.8	Avg.	St.dev.
A_{k_c}	−0.37	−0.46	−0.48	−0.51	−0.36	−0.48	−0.33	−0.34	−0.42	0.07
B_{k_c}	4.07	4.21	4.22	4.27	4.09	4.21	4.02	4.06	4.14	0.09
A_{AE}	−0.92	−0.87	−0.88	−0.91	−0.77	−0.81	−0.81	−0.71	−0.84	0.07
B_{AE}	2.61	2.56	2.55	2.56	2.41	2.50	2.48	2.38	2.51	0.08